ACS NANO
www.acsnano.org

Graphene Tunable Transparency to Tunneling Electrons: A Direct Tool To Measure the Local Coupling

Héctor González-Herrero,[†,‡] Pablo Pou,[‡,§] Jorge Lobo-Checa,[∥] Delia Fernández-Torre,[§] Fabian Craes,[⊥] Antonio J. Martínez-Galera,[†,⊥] Miguel M. Ugeda,[#,∇] Martina Corso,[∥,∇] J. Enrique Ortega,[∥,¶,○] José M. Gómez-Rodríguez,[†,‡] Rubén Pérez,[‡,§] and Iván Brihuega*[,†,‡]

[†] Departamento de Física de la Materia Condensada, Universidad Autónoma de Madrid, E-28049 Madrid, Spain

[‡] Condensed Matter Physics Center (IFIMAC), Universidad Autónoma de Madrid, E-28049 Madrid, Spain

[§] Departamento de Física Teórica de la Materia Condensada, Universidad Autónoma de Madrid, E-28049 Madrid, Spain

[∥] Centro de Física de Materiales (CSIC-UPV-EHU) and Materials Physics Center (MPC), Manuel Lardizábal 5, E-20018 San Sebastián, Spain

[⊥] II. Physikalisches Institut, Universität zu Köln, Zülpicher Straße 77, 50937 Köln, Germany

[#] CIC nanoGUNE, 20018 Donostia-San Sebastian, Spain

[∇] Ikerbasque, Basque Foundation for Science, 48013 Bilbao, Spain

[¶] Donostia International Physics Center DIPC, E-20018 San Sebastián, Spain

[○] Departamento de Física Aplicada I, Universidad del País Vasco, E-20018 San Sebastián, Spain

Supporting Information

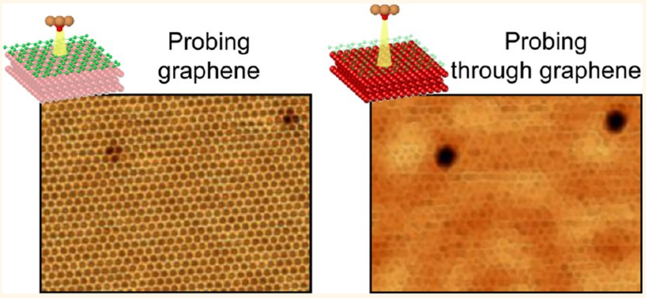

ABSTRACT: The local interaction between graphene and a host substrate strongly determines the actual properties of the graphene layer. Here we show that scanning tunneling microscopy (STM) can selectively help to visualize either the graphene layer or the substrate underneath, or even both at the same time, providing a comprehensive picture of this coupling with atomic precision and high energy resolution. We demonstrate this for graphene on Cu(111). Our spectroscopic data show that, in the vicinity of the Fermi level, graphene π bands are well preserved presenting a small n-doping induced by Cu(111) surface state electrons. Such results are corroborated by Angle-Resolved Photoemission Spectra (ARPES) and Density Functional Theory with van der Waals (DFT + vdW) calculations. Graphene tunable transparency also allows the investigation of the interaction between the substrate and foreign species (such as atomic H or C vacancies) on the graphene layer. Our calculations explain graphene tunable transparency in terms of the rather different decay lengths of the graphene Dirac π states and the metal surface state, suggesting that it should apply to a good number of graphene/substrate systems.

KEYWORDS: *graphene, Cu(111), electronic properties, STM, DFT, ARPES*

Graphene is known to exhibit notable differences in its electronic properties on top of different substrates. This is a consequence of the specific coupling between the graphene layer and its underlying host. A collection of exciting properties such as band structure gaps, n- and p-type doping, magnetism, changes in Fermi velocity, or superconducting behavior have been found by choosing appropriate substrates.[1−10] Moreover, graphene−substrate interaction can be further modified by the intercalation, incorporation, or adsorption of additional material. They locally induce gaps in the band structure of graphene, magnetic moments, or decouple electronically the graphene layer.[11−18]

Gaining a detailed knowledge of the graphene−substrate coupling would make possible not only to characterize any novel property, but also to envision and design further ways of incorporating additional capabilities. Hence, a great experimental and theoretical effort is currently involved in

Received: January 14, 2016
Accepted: April 25, 2016
Published: April 25, 2016

DOI: 10.1021/acsnano.6b00322
ACS Nano 2016, 10, 5131−5144

measuring, understanding, and controlling such interactions. From the experimental side, macroscopic techniques, such as ARPES or X-ray Photoemission (XPS), can provide overall information about both the characteristics of the graphene layer and the underlying substrate,[2,8,17,19,20] but lack the local resolution required to explore in detail the coupling of specific graphene regions. Local experimental techniques, such as STM or High-Resolution Transmission Electron Microscopy (HRTEM), can, on the other hand, characterize with atomic precision any modification on the graphene layer,[12,14,21−26] but to date have provided very limited information about the underlying substrate. Such information is key to understand in depth the interactions on the local scale. It is noteworthy that a few STM works have already indicated that under certain conditions the graphene layer is not visible in tunneling experiments, which directly probe the underlying substrate.[27−32] From the theoretical side, calculations are rapidly progressing to understand this coupling, but to reach the insight required in the modelization, a complete experimental data set is necessary to ensure the consistency of the theory. In such weak graphene−substrate interaction systems, the used functionals must be further optimized to accurately include van der Waal forces.

In this work, we aim to demonstrate the potential of graphene tunable transparency to probe local interactions by thoroughly characterizing the graphene−Cu(111) coupling using STM and Scanning Tunneling Spectroscopy (STS) experiments. Our approach consists in selectively modifying the STM tip apex and/or the tunnel parameters to locally visualize, in the same energy range, either the graphene layer or the copper surface underneath, or even both at the same time. Our results, supported by ARPES and state of the art calculations (Density Functional Theory with van der Waals, DFT + vdW), yield a detailed picture of the existing electronic interactions and offer a clear explanation for the transparency mechanism. We have chosen graphene on Cu(111) as a model system to understand graphene tunable transparency for three main reasons: (i) It has a very weak graphene−metal interaction, which allows us to obtain the electronic properties of the graphene layer by visualizing the graphene quasiparticle dispersion. (ii) The Cu(111) surface is a well-characterized substrate, so any modifications on its surface states induced by the interaction with the graphene layer can be easily identifiable. (iii) Graphene on Cu is a very attractive system for practical applications since it enables the growth of high quality graphene films due to the low solubility of carbon in Cu[33] and can be transferred onto arbitrary substrates by chemical etching of the underlying metal.[34,35]

In addition, we show that this graphene tunable transparency can also be used to locally probe the interactions that adsorbates generate on the system. Structural or chemical modifications are frequently introduced to graphene layers to selectively modify its properties,[11,12,14] but whether these properties will remain in the presence of an underlying substrate is a crucial but far from trivial question that needs to be solved for each specific system. In fact, even if the properties of graphene are weakly affected by a specific substrate, local modifications of the pristine graphene layer can noticeably modify its coupling to the substrate. This has been shown for the weakly interacting graphene/Pt(111) and graphene/Ir(111) systems, where the interaction with the graphene layer strongly increases after the introduction of single carbon vacancies in the graphene layer[36] or by the adsorption of H or Ir atoms.[11,37] According to theoretical predictions, a strong local interaction between the graphene and substrate develops where the vacancies or atomic adsorbates are located. Of particular interest is the adsorption of atomic hydrogen on graphene. It is known to induce exciting changes in the electronic properties of isolated graphene,[38−40] and for the graphene/Ir(111) system, it was reported to give rise to the opening of a band gap in graphene due to a strong increase of the graphene−metal interaction at H sites.[11] Hence, as a proof of principle, we investigate atomic hydrogen adsorbed in our graphene/Cu(111) system and single C vacancies deliberately introduced on the graphene layer to show that graphene tunable transparency can reveal the local interactions between adsorbates with both the graphene layer and the substrate underneath.

RESULTS AND DISCUSSION

Due to its weak interaction, graphene usually grows on Cu(111) in several orientational domains, which leads to the formation of moiré patterns with different periodicity (see Figure 1, Figure S1, and Methods section).[31,41,42] Such large, periodic domains can be easily located and characterized by STM and STS. Our methodology is illustrated in Figure 1, where we focus our attention into one such domain and image it using two different tip apex terminations but with identical scanning conditions. Because of graphene's tunable transparency to tunneling electrons, we can selectively visualize only the graphene layer as in Figure 1a, or tunnel through such overlayer revealing the modifications induced on the Cu(111) surface by the coupling with graphene as in Figure 1b. Such changes in the tip visualization mode are fully reversible and are deliberately introduced by controlled indentations of the STM tip onto the G/Cu(111) substrate (see Methods for details).

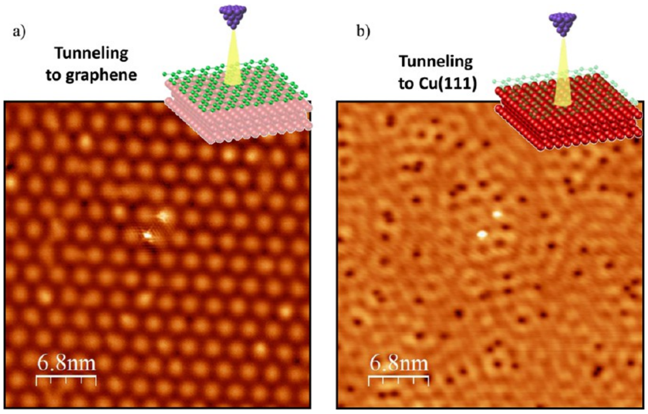

Figure 1. STM images showing the same graphene/Cu(111) sample region measured with different tip apex terminations, which enables us to selectively visualize in the same energy range, graphene (a) or the Cu(111) substrate underneath (b). Image size, 34 × 34 nm^2; sample bias, 50 meV; tunnelling current, 0.4 nA.

When tunneling into the graphene layer (Figure 1a), STM images show the structural overlayer conformation, *i.e.*, the honeycomb carbon lattice (see Figure S2) and the moiré pattern. From this, we can infer the actual rotation between the graphene and the Cu(111) surface (25° in Figure 1). In addition, by measuring dI/dV maps as a function of energy, one can also visualize the energy dependence of the quantum interference patterns originated by the scattering of graphene

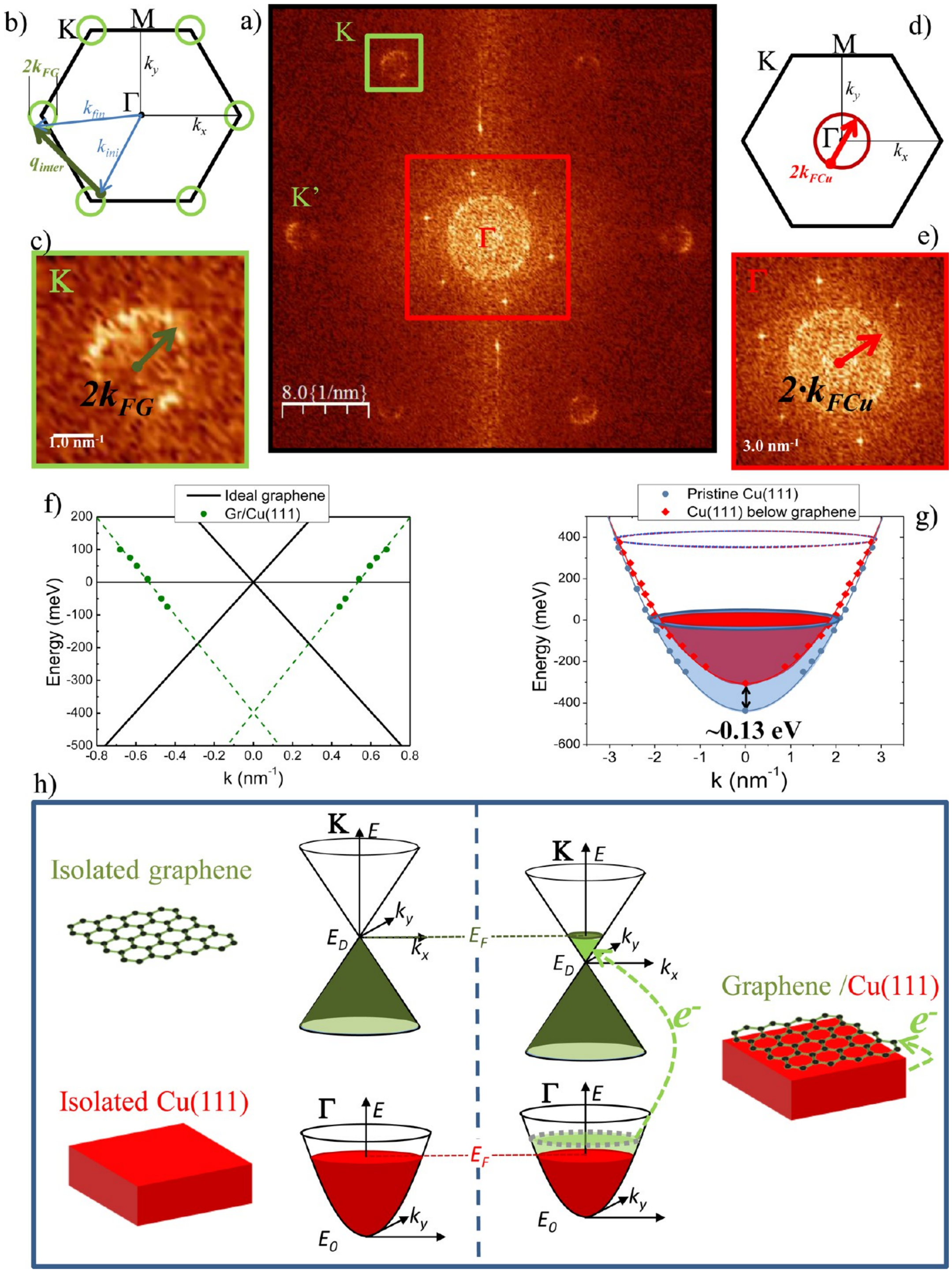

Figure 2. Electronic structure of the Gr/Cu(111) system by LT_STM. (a) 2DFT of the LDOS measured at E_F on a 45 × 45 nm^2 graphene/Cu(111) region, when the tip is tuned to visualize both graphene and Cu underneath (real space in Figure S3). (b) Schematic Fermi surface for electron-doped graphene, where arrows illustrate an elastic intervalley scattering process. (c) Zoom-in on the outer ring centered at *K* point outlined in (a) by the green square. (d) Schematic Fermi surface of the Cu(111) surface state. (e) Zoom-in on the central region outlined in (a) by the red square. The bottom left panel corresponds to the STM experimental electronic characterization of graphene on Cu(111). The energy dispersion of graphene π bands (f) is obtained from the energy dependence of the radius of the ring like features centered at *K* points of the Brillouin zone. (g) Comparison between the energy dispersion of the Shockley surface state of pristine Cu(111) (blue data) and of Cu(111) below graphene (red data). (h) Schematic summary of the electronic charge transference extracted from our STM measurements. Left panel corresponds to the band structures of isolated graphene and Cu(111). Right panel indicates the changes in the band structures induced by the graphene/Cu(111) coupling.

quasiparticles. This provides with great accuracy the dispersion of the graphene π bands in the vicinity of the Fermi energy (E_F). Since the characterization of 2D electronic states by STM is of particular interest for the present study, a comprehensive discussion about it can be found in the Supporting Information. In the case of graphene, the low energy bands consist of cones

DOI: 10.1021/acsnano.6b00322
ACS Nano 2016, 10, 5131−5144

Table 1. Parameters Obtained for STM, ARPES, and DFT + vdW for the Cu(111) Surface State on the Pristine Surface and Graphene Covered[a]

	STM (5 K)		ARPES (180 K)		DFT + vdW		
	Cu(111)	Cu(111) below graphene	Cu(111)	Cu(111) below graphene	Cu(111)	Cu(111) below graphene (3.4 Å)	Cu(111) below graphene (2.9 Å)
E_0 (meV)	−430 ± 10	−300 ± 10	−400 ± 10	−263 ± 10	−390	−260	0
m^*/m_e	0.39 ± 0.01	0.43 ± 0.01	0.41 ± 0.01	0.43 ± 0.01	0.38	0.41	0.48
k_F (nm^{-1})	2.10 ± 0.05	1.80 ± 0.04	2.05 ± 0.05	1.75 ± 0.05	1.97	1.70	0

[a] Notice that the temperatures for STM and ARPES are different, which translates in a rigid shift of the parabola towards E_F as the temperature is raised.[63,64]

at K and K' points of the Brillouin zone, named valleys, presenting a linear and isotropic dispersion. Accordingly, near E_F, graphene constant-energy contours correspond to rings of radius $k(E)$ centered at the K and K' points of the Brillouin zone, see Figure 2b. In monolayer graphene, due to the peculiar symmetry of quasiparticle wave functions, named pseudospin, two-dimensional Fourier Transform (2D-FT) of dI/dV maps essentially probe intervalley scattering processes.[43,44] As depicted in Figure 2b, in those events graphene quasiparticles scatter between neighboring valleys, giving rise to scattering vectors $q(E)$, which correspond to $(\sqrt{3} \times \sqrt{3})$R30° interference patterns in the local density of states (LDOS). Thus, our 2D-FT (Figure 2a,c) shows ring-like features of radius $2k(E)$ centered at K and K' points of the Brillouin zone.

By selecting the appropriate tunneling conditions, one can simultaneously image both the graphene layer and the underlying Cu(111) substrate. This is shown in Figure 2a presenting the 2D-FT of the LDOS measured at E_F on a 45 × 45 nm^2 G/Cu(111) region. Scattering processes from graphene quasiparticles give rise to the aforementioned K and K' rings (green square), whereas scattering processes from Cu(111) surface quasiparticles generate the central, larger ring visible at Γ (red square). As shown in Figure 2c,e, the radius of the rings centered at K/K' and Γ points correspond to twice the Fermi wave-vector of the graphene layer and the underlying Cu(111) surface state, respectively. In the 2D-FT central zone, outlined by the red square, six points show up due to the moiré pattern originating from the existing rotation of 12° between the graphene layer and the Cu(111) surface.

The dispersion of both the graphene Dirac-like band and the Cu(111) surface state can be obtained from the 2D-FT in energy dependent dI/dV maps, see Figure 2, panels f and g, respectively. A linear dispersion characterized by $k_{FG} = 0.54$ nm^{-1} and $v_{FG} = 1.1 \times 10^6$m/s is obtained for graphene in the present case, see Figure 2f, Figure S5, and Table 2. Our STS data show an upward shift of +0.13 eV on the onset of Cu(111) (see also dI/dV spectra in Figure S5d). Aside from this energy shift, the energy dispersion obtained from the 2D-FT of dI/dV maps shows a nonrigid upward displacement of the Cu(111) surface state band, with an effective mass increase from $0.39m_e$ to $0.43m_e$ (Figure 2g and Table 1). In Figure S5f, we superimpose the central region of the 2D-FT of dI/dV maps measured at E_F on covered and uncovered Cu(111) regions. A smaller ring, corresponding to a smaller Fermi wave-vector in graphene covered areas, indicates the electron depletion of the Cu(111) surface state band. Earlier STM/STS experiments[45,46] have reported similar modifications of the Cu(111) surface state in the presence of weakly interacting overlayers, such as 1 ML Xe or insulating NaCl, whose very low DOS at E_F enables the transparency of tunneling electrons.

Figure 2h qualitatively sketches the outcome of our measurements. A graphene Fermi wave-vector of $k_{FG} = 0.55$ nm^{-1} is found in revealing an electron doping of 1.0×10^{-3} e/Å^2 for the overlayer (the Dirac point is exactly at E_F, *i.e.*, $k_{FG} = 0$, for isolated graphene). This graphene doping is due to an electronic transfer from the Cu(111) surface state, whose Fermi wave-vector decreases from the value of $k_F = 2.10$ nm^{-1} of the pristine Cu(111) surface, to $k_{FCu} = 1.80$ nm^{-1}, found in the presence of the graphene overlayer (see Figure S5f for a direct comparison). As explained later, not all the charge leaving the Cu(111) surface state is incorporated into the graphene layer. It is noteworthy that the STM values have been obtained from over 50 graphene and Cu(111) regions exhibiting different orientations where practically identical doping level values are found (see details in Supporting Information and Figure S8). Such constant experimental doping for the graphene−Cu(111) interface suggests that graphene doping is dominated by the nature of the underlying substrate with little influence of the specific arrangement of the graphene layer.

To shed light on the graphene−metal interaction, first-principles calculations based on recent improvements on density functional theory (DFT) that include dispersion interactions[47,48] have been extensively used.[49] Although they have disclosed some of the fundamental properties of these systems, some theoretical approaches have not been conclusively validated. Main concerns lay on the vdW interactions. Approaches for dispersive interactions have been well tested for molecule−molecule interactions or the absorption of small molecules on surfaces where more exact methods can be used.[47,48] However, on extended systems, their size prevents the use of these accurate methodologies, so the validation of the theoretical results has to come exclusively from the comparison with experimental data. Graphene on metals is a prototypical example of extended system ruled by vdW-interactions. There are already multiple references where DFT + vdW simulations in G−metal systems have been compared with the data measured with different structural and spectroscopic experimental techniques.[50] The experimental findings presented above, exploiting the tunable transparency, offer the quantitative information needed to further refine that comparison on several key parameters that characterize the G−metal coupling such as the G layer−metal distance, the graphene corrugation and the charge transfer within a single experimental technique. For example, in the absence of a precise determination of the G−Cu distance using XRD methods, the strong distance dependence of the changes induced in both the G and the Cu surface state has allowed us to determine the G−metal separation, a parameter controlled by the attractive vdW interactions. Thus, our approach, which can be extended to other G−metal systems, offers the possibility to test and eventually tune the theoretical approaches and, in this way,

DOI: 10.1021/acsnano.6b00322
ACS Nano 2016, 10, 5131−5144

achieve a comprehensive accurate description of the metal−graphene interaction.

We have used this experimental information to test the description of the G/Cu(111) interaction provided by first-principle simulations that combine DFT with different theoretical approaches to describe vdW interactions. These methodologies include the use of the PBE[51] exchange-correlation (XC) functional supplemented by semiempirical approaches like the popular Grimme D2[52] (PBE-D2) and Grimme D3 (PBE-D3),[53] and recently proposed functionals that include the vdW interactions in the XC kernel (DFT-DF), like the optB86b-vdW functional proposed by Klimes *et al.* (see Supporting Information).[54] For all these calculations, we have used the VASP code[55] with a 400 eV cutoff for the plane wave basis set and PAW pseudopotentials (see the Methods section for details).[56] The experiments show that the Cu surface state plays an important role on this system. An accurate description of this state with DFT simulations requires a slab with more than ∼15 Cu layers in order to decouple the surface states of both slab faces. Using a Cu slab consisting on a 1 × 1 surface cell and 15 layers, we obtain the onset of the surface state at about −0.39 eV with respect to the Fermi level and an effective mass m^*/m_e of ∼0.38, in good agreement with our STM experiments and previous calculations. The addition of the graphene layer to the 1 × 1 Cu(111) slab (see Methods and Supporting Information for further details) results on a charge transfer between the graphene and the metal that shifts the Dirac point toward lower energies.[57] The graphene−metal attraction is essentially provided by the vdW interaction: a calculation without the dispersion forces results on much larger graphene−Cu distance and a very small binding energy. As discussed below, we have also considered calculations with the observed $\sqrt{57} \times \sqrt{57}$ moiré periodicity (Figure S10) on a 4-layer Cu slab, which show that the changes induced by the presence of the graphene layer are in agreement with those obtained in the (1 × 1) 15-layer Cu slab.

Our PBE-D2 calculations yield a graphene−surface average distance of ∼2.9 Å, which translates into an unrealistic downward shift of the Dirac point of ∼0.65 eV and an upward shift of the onset of the Cu surface state of ∼0.4 eV with an effective mass of m^*/m_e of ∼0.48 (see Figure 3c,d and Tables 1 and 2). The comparison of these numbers with the local STM experimental information indicates that the charge transfer yielded by the simulation is much larger than the real one, *i.e.*, the PBE-D2 method is overestimating the graphene−metal interaction. In the calculations, this interaction can be easily tuned modifying the graphene−metal surface distance. In this way, we have obtained a clear correlation between the shifts of the Dirac point and the onset of the Cu surface state with respect to the graphene−Cu distance, see (Figure 3d). At an average distance of 3.4 Å, with an energy increase of just 45 meV per surface unit cell (with respect to 2.9 Å), the shift of the onset of the Cu surface state is +0.13 eV with an effective mass of $m^*/m_e \sim 0.41$ and the Dirac point is placed at −0.35 eV with $k_{FG} \sim 0.6$ nm^{-1}, all in excellent agreement with the experiments, see Figure 3 and Table 2 (notice that for the separation of 2.9 Å we get an unrealistic value of $k_{FG} = 1.3$ nm^{-1}).

Our calculations show that while the total binding energy, essentially controlled by the vdW forces, is quite flat, the resulting graphene−metal coupling, reflecting the overlap of the wave functions and described by DFT, strongly depends on the graphene−metal distance. From the comparison between theory and experiments, we can conclude that the graphene−metal coupling is correctly described by PBE at the 3.4 Å G−Cu distance. We have cross-checked our calculations using a larger $\sqrt{57} \times \sqrt{57}$ moiré pattern with respect to the graphene (Figure S10). Our calculations show that the link between graphene−metal distances and energy shifts are essentially the same for the more realistic $\sqrt{57} \times \sqrt{57}$ moiré pattern and the 1 × 1 surface cell, and, thus, validate our previous discussion on the properties of both graphene and the Cu surface state and their interaction. The discrepancies with the experiments can be indeed attributed to details in the description of the vdW interactions: Our calculations show that more accurate approaches like PBE-D3[53] and the DFT-DF optB86b-vdW functional[54] yield G−Cu distances of ∼3.2 and ∼3.3 Å, respectively (see Figure 3d and Supporting Information for details).

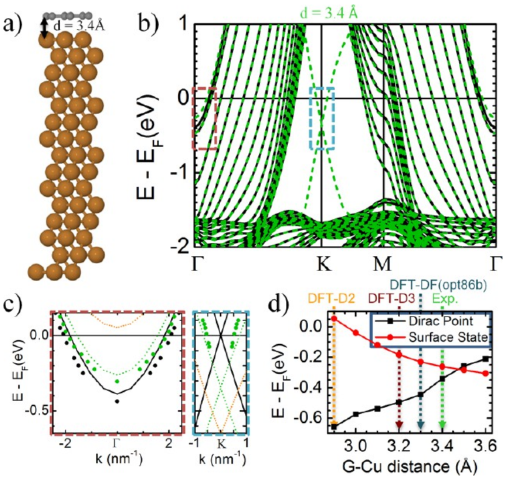

Figure 3. DFT + vdW calculations of the G/Cu(111) system. (a) Ball-and-stick model of the (1 × 1) surface cell of graphene on Cu(111). (b) Band structure of graphene on Cu(111) for the (1 × 1) surface cell with optimal empirical graphene−Cu distance of 3.4 Å (green dashed lines) and the isolated Cu slab bands (black lines). (c) Zooms of the G/Cu (green dashed lines) and Cu (black lines) bands in the vicinity of E_F around Γ and K high symmetry points, which include the experimental results (dots). For comparison, the bands for a 2.9 Å graphene−Cu separation (orange dot lines) are included. (d) The graphene Dirac point (black line) and the Cu surface state (red line) positions as a function of the G−Cu distance. The equilibrium distances obtained with DFT-D2 (orange), DFT-D3 (purple), DFT-DF(opt86b) (blue) and the optimal empirical G−Cu (green) separations are marked.

This accurate description allows us to provide more trustful quantitative information on the graphene−Cu coupling. Aside from doping, we find that the graphene bands close to E_F practically do not interact with Cu bands keeping unmodified the graphene electronic properties (see Figure 3b). This doping is due to both work function differences of Cu and free-standing graphene (∼0.2 eV) and the interaction between them[57] (see Figure S9). Our experiments show that the graphene is increasing its electronic charge by 1.0 × 10^{-3} e/Å^2, while the Cu surface state is transferring 1.9 × 10^{-3} e/Å^2. This suggests the presence of a charge dipole pointing from the G to the Cu. However, the decrease in the work function of the G/Cu, 4.3 eV in our calculations (4.2 eV measured with ARPES), with respect to the Cu(111) surface, ∼4.8 eV (4.9 eV measured with ARPES) requires a dipole in the opposite direction.[57] This dipole can be clearly observed in Figure S9, where the

Table 2. Parameters Obtained for STM, ARPES, and DFT + vdW for the Graphene π Bands of the Graphene Layer on the Vicinity of the K and K' Points[a]

	graphene on Cu(111)			
	STM (5 K)	ARPES (180 K)	DFT + vdW (3.4 Å)	DFT + vdW (2.9 Å)
E_D (meV)	−400 ± 20*	−380 ± 10	−350	−650
v_F (m/s)	$(1.1 \pm 0.1) \times 10^6$	1.0×10^6	0.89×10^6**	0.76×10^6**
k_F (nm^{-1})	0.55 ± 0.03	0.60 ± 0.06	0.6	1.3

[a] *E_D value from STM data is estimated from the linear fit of STS data near E_F; see green dotted line in Figure 2f. **Graphene strain and e−e interactions could slightly affect calculated v_F values.

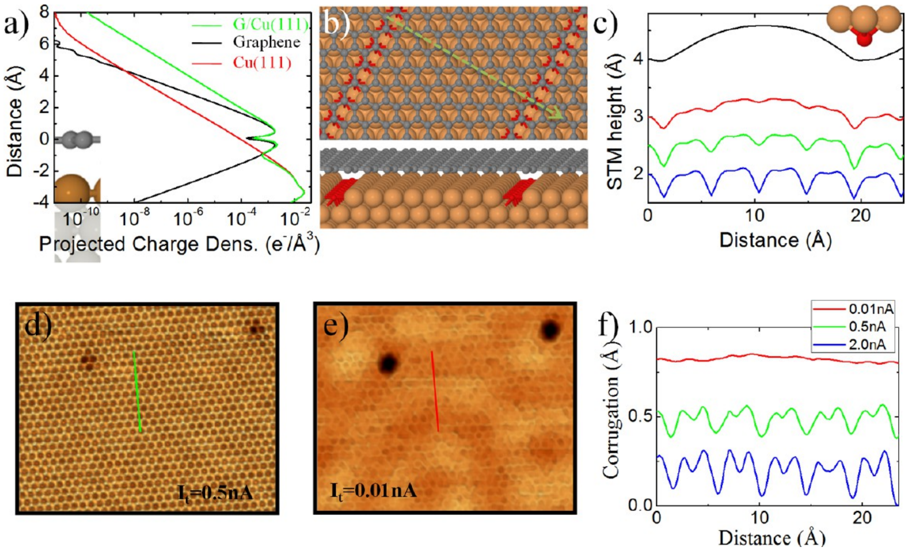

Figure 4. STM simulations and explanation for the tunable transparency of the graphene overlayer. (a) Projected charge density on the energy range from −0.5 eV to E_F integrated in the xy plane as a function of perpendicular position for graphene on Cu (green line), for a Cu(111) slab (red line) and for an isolated graphene (black line). Note that all curves share the same relative positions, and graphene is its distance origin. We observe that the Cu surface state decay length is larger than graphene, so for graphene on Cu, the charge at larger distances is dominated by Cu. (b) Stick-and-ball model of the atomic configuration of a graphene layer on a Cu surface tailored with an oxygen row substituting Cu surface atoms in order to create a spatial modulation of the Cu surface state (see Methods). (c) Simulated constant current STM profiles along the green line marked on (b) at different tip sample separations and at a −0.1 V bias (the STM height is defined respect to the z coordinate of the carbon atom, at distance = 0 Å). The bottom panels correspond to experimental data that agrees exceptionally well to the simulations: (d and e) show experimental constant current STM images at two different current set points (I = 0.5 nA and I = 0.01 nA, respectively); (f) compares the same line profile (outlined by the green and red line in (d) and (e)) at different constant current set points. Notice that both experimental and simulated STM profiles show the Cu surface state modulation at larger tip−sample distances, while the graphene atomic contrast is disclosed for closer tip−graphene separation.

calculated plane-averaged differential electron density is represented.

Our results concerning the nature (n-doping) and distance dependence of the charge transfer to graphene from Cu are consistent with earlier calculations by Giovanetti *et al.* using the local density approximation (LDA) to the exchange correlation functional[5] and later work from some of those authors[57] using the PW91 GGA functional. Our calculations also reproduce the prediction of ref 5 of an interface dipole that tends to reduce the work function of the G/Cu system with respect to that of the clean metal. However, the orientation of this dipole (see Figure 5 in ref 57), with the positive charge close to the G sheet seems to be inconsistent with the G being n-doped (extracting electrons from the metal). Our detailed measurements of the Fermi wave vectors of G and the Cu confirm that this is indeed the case and identify one important contribution to the G doping, with electrons being transferred from the surface state to G. The way out of this puzzle is to abandon the naive view of charge being transferred and localized at the positions of the atoms and focus instead on the spatial extension of the electronic orbitals involved in the process. The Cu surface state extends through and beyond the G and its loss of charge in that area is larger than the charge gained by the pure G states, that are significantly more localized. The 0.9×10^{-3} e/Å^2 of the charge left by the Cu surface state, which is not incorporated into the graphene layer, is located on the G−Cu coupling area to complete the dipole. The large extension of the Cu surface state (illustrated in Figure 4a) is not only important to explain the puzzle between n-doping and the interface dipole, but provides the crucial hint to understand the tunable transparency of G, as discussed in the following. The previous analysis has been possible due to the experimental ability to sense both the graphene and the substrate underneath. It is of paramount importance to understand the mechanism behind this graphene tunable transparency. The answer lies in the difference in the decay lengths between the metal surface state and the graphene π-states, much larger in the first case. To demonstrate this, we present in Figure 4a the calculated plane-averaged electron density projected on the energy range −0.5 eV to E_F (see Figure S11 for calculations of a broader energy range) for an isolated Cu slab (red line), a free-standing graphene layer (black line), and both together with the optimal separation of 3.4 Å (green line). The decay of the Cu surface state is slow compared to the graphene, which shows a more localized charge in space. For distances larger than ~4 Å from the graphene, the charge density coming from the Cu is prevailing over that of the graphene even though the metal surface is 3.4 Å deeper. The π-G states are more localized than the Cu surface state by both the in-plane wave vector of the electronic states and the out-of-plane extension of the atomic orbitals. Following a simple model, the main dependence of the STM current with the distance for a given state can be approximated by $I \sim \exp(-2(k^2_{\mathrm{wf}} + k^2_{\parallel})^{1/2}d)$,[58] where k_{wf} is the inverse of the decay length of the wave functions and $k_{\parallel}$ is the in-plane wave vector of the states. The k_{wf} associated with the carbon π orbitals is larger than the one associated with the very spatially extended Cu surface states. Moreover, the $k_{\parallel}$ associated with the Cu surface state is small as the band is centered around Γ, while for the relevant G states, centered around K, it should be of the order of the size of the Brillouin Zone $k_{\parallel} \sim 1.3$ Å^{-1}. Therefore, the contribution to tunneling of the G states with respect to the Cu surface state band is quickly reduced upon increasing the tip−sample separation. In the case of the graphene/Cu system (green line of Figure 4a), the charge density distribution is modified by the charge transfer and the change in electrostatic potential. This induces an extension of the Cu density which dominates even 3−4 Å above the graphene. Note that the decay length for the G/Cu system and the clean Cu slab are equal, but with an effective displacement of ~2 Å induced by the graphene layer. Such wave function spill-out restricts the conditions for atomic resolution in graphene to tip−sample distances less than 3−4 Å where the tip apex is really close to the G overlayer, while local variations on the Cu surface can be observed at larger tip−surface distances. The large tip−sample forces developed under these operation conditions prevent stable scans with reactive tips apexes, like those of purely metallic tips. Only weakly interacting tips, with apexes passivated with electronegative atoms, can provide atomic resolution on G on Cu.

To substantiate these simple arguments and to identify the nature of the tips that allow the imaging of both G and the Cu surface state, we have combined our first-principles simulations with Non Equilibrium Green Function calculations[59] to determine the electronic current between the STM tip and the G/Cu(111). A simulation of the Cu surface standing waves observed on the STM experiments, created by the scattering of a low density of point defects and extending for several nanometers, would require extremely large cells. To capture this effect with a reasonable use of computational resources, we have introduced an artificial electronic modulation on the Cu surface with a line defect: we replace an entire row of Cu surface atoms on the $[1\bar{1}0]$ direction by oxygen atoms, and repeat this process with a periodicity of ~2 nm, large enough to accommodate the lateral decay of the real standing waves. This can be simulated with a 9 × 1 surface cell and a slab that includes the 15 Cu layers required to properly describe the Cu surface state. We also include the G layer at the distance of 3.4 Å following a 1 × 1 moiré pattern (see Figure 4b and Methods for details).

In the experiments, we have found two different kinds of tips. After preparation by soft contact with the G/Cu(111) substrate, see Methods for details, most of the tips easily image the Cu standing waves, but only few are able to provide atomic resolution on G. While working with these last tips, we discovered that a reduction on the set point (an increase of the tip−surface distance) resulted on a change of contrast from the graphene to the Cu.

To understand this behavior, we have theoretically analyzed the STM contrast obtained with two different models for tip apexes: A pure Cu (111)-oriented tip with 10 atoms (Cu10 tip), and a O-contaminated tip, where we replace the Cu atom at the apex by an O atom (CuO tip). Both structures are stable and we have used them in previous studies of STM/AFM imaging on $\mathrm{CuO_2}$ surfaces.[60] In the context of the G/Cu system, the O atom mimics the possible contamination of the tip with electronegative impurities with similar chemical properties, like S, that are known to be abundant in Cu[31,61] and thought to be a local source of scattering that contributes to the observed standing wave pattern. Note that metal tips are very reactive and thus prone to contamination.

Figure 4c shows simulated constant current STM line profiles, along the green line indicated on Figure 4b and including multiple scattering effects,[59] for four tip−surface distances, calculated using the CuO tip. At $d = 4$ Å (black line), only the modulation induced by the defects on the Cu surface is observed. Upon tip approach, atomic corrugation in the G is obtained, while the electronic modulation of the Cu surface gets reduced, becoming negligible at $d = 2$ Å. This is precisely the observed experimental behavior displayed in Figure 4d−f, acquired with the same nonreactive tip, on the very same sample region, and at different constant current set points (2.0, 0.5, and 0.01 nA). For higher currents, corresponding to smaller tip−sample distances, the STM essentially visualizes the graphene honeycomb, whereas for lower currents, *i.e.*, larger tip−sample distances, standing waves from the Cu(111) surface state become dominant.

Figure S12 compares constant height profiles calculated with the purely metallic Cu10 tip and the contaminated CuO tip. At large distances ($d > 4$ Å), both tips are sensing the charge modulations originated in the Cu surface states by defects on its surface, confirming the key role of the different decay lengths of Cu surface states and G π states in the imaging of the Cu substrate, that almost any tip is able to capture. At closer distances ($d = 3$ Å), the contrast of the Cu tip is still dominated by the metal states, while there are already clear features that reveal atomic contrast in G. We have seen a similar effect in oxide surfaces, where both Cu and O atoms are present in the outmost layer, and only CuO tips are able to image the rather localized states on the O atoms.

For close enough distances, the Cu tip, as representative of any metal tip, would also show atomic contrast on G, but we can discard it as a suitable candidate to explain the experiments for two reasons: (i) the interaction of the Cu tip with the substrate is very strong, particularly at the rather small surface distances required to get atomic resolution on G ruling, making stable operation very challenging; (ii) in that short distance range, due to multiple scattering effects,[62] those metal tips would provide an inverted contrast image with hexagonal (not honeycomb) symmetry, where the maxima of the current are on the hollow sites not on the atoms.

In essence, the excellent agreement between experiments and simulations validates our explanation for the transparency of the STM on graphene on metal in terms of the extension of the metal surface state *versus* the spatial localization of the graphene charge density in the normal direction, and allows us to identify a metal tip contaminated with electronegative species as

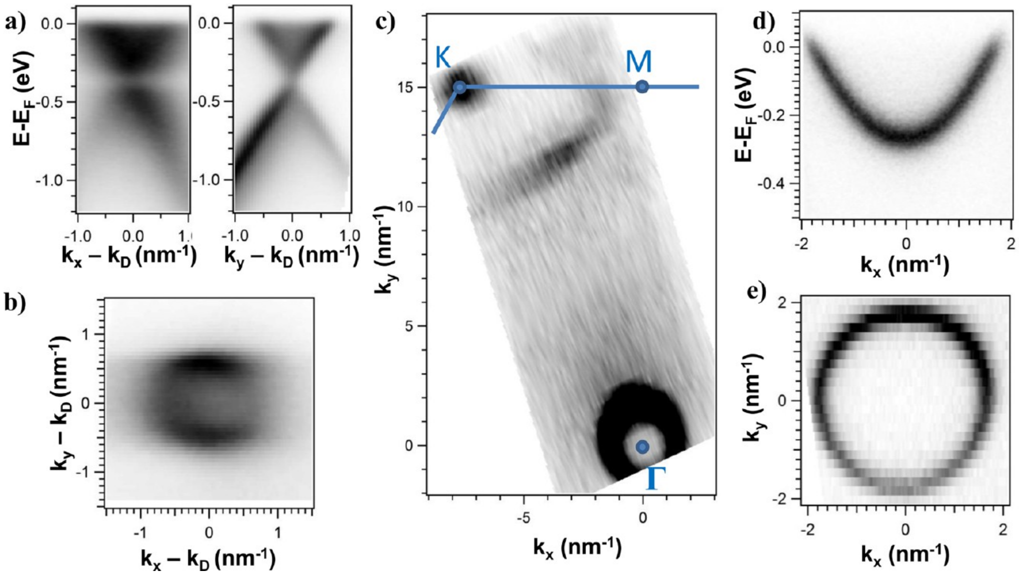

Figure 5. Experimental electronic structure of graphene on Cu(111) as obtained from ARPES. The raw data is represented in grayscale, where darker tones represent higher intensity. It clearly shows the graphene π band around the *K* point (panels a and b) as well as the modified Cu(111) Shockley state in the proximity of the Γ point (panels d and e). Panel c presents a section of the Fermi surface where the blue line shows the edge of the Brillouin zone and relevant high-symmetry points. The feature away from the high-symmetry points (close to 11 nm^{-1}) corresponds to the Fermi energy crossing of the Cu sp-bulk band. The graphene π band is scaled in reference to the Dirac point position (found at E_B = 0.38 eV and $k_{\parallel}$ = 16.8 nm^{-1}). The Shockley state is symmetric around Γ with a rigid shift of ~140 meV when compared to pristine Cu(111) (panels d and e). The ARPES data was acquired at 180 K using a monochromatized UV lamp ($h\nu$ = 21.2 eV).

representative of the experimental tips that are able to image both the Cu substrate and the G honeycomb lattice.

Our calculations show that to access the electronic properties of graphene by STM we need a weakly reactive tip enabling operation at small tip–sample distances. It is important then to rule out any spurious influence of the STM tip in our data. To this end, we have performed additional ARPES experiments. Fermi surfaces and band dispersions close to the center (Γ) and edge (*K*) of the Brillouin Zones are readily probed, as shown in Figure 5. ARPES is highly complementary to STM since it measures in the reciprocal space and therefore has direct access to the electronic structure of the system (no 2D-FT required). The important differences with STM are that only the DOS of the sample are probed (no tip involved) and ARPES averages over the whole illuminated region (nonlocal technique). The main drawback is that ARPES demands an excellent surface preparation, in order to achieve homogeneous, single domains extending over large sample areas. This is indeed the case of our samples: the data in Figure 5 indicate the presence of a dominant graphene domain orientation over the area sampled by the light spot size of 0.25 mm^2.

The Fermi surface portion displayed in Figure 5c shows both the graphene π bands surrounding the *K* point and the modified Cu(111) Shockley state around the Γ point. Zoom-out views at both symmetry points are shown in Figure 5, panels b and e, whereas the respective band dispersions are shown in Figure 5, panels a and d. The excellent agreement with the STM and DFT + vdW results shown in Tables 1 and 2 excludes any tip-influence in our measurements confirming graphene tunable transparency as an ideal tool to probe graphene–substrate interactions.

One of the mayor strengths of this method stems from its ability to locally probe such interactions. In this way, graphene tunable transparency can be further exploited as an extraordinary tool capable of tracking additional local interactions introduced in the system. As a case example, one could consider the adsorption of dilute atomic hydrogen on G/Cu(111) and the introduction of C vacancies in the graphene layer.

It has been reported that atomic H on isolated graphene layers induces exciting changes in the electronic properties, such as the opening of band gaps[40] or the generation of local magnetic moments.[38,39,65] For the weakly interacting G/Ir(111) system, it was reported that it gave rise to the opening of a band gap in graphene due to a strong increase of the graphene–metal interaction mediated by the local rehybridization of C atoms from sp^2 to sp^3 bonding, with H binding on top of a C atom as in the isolated graphene layer and the surrounding C atoms binding to an Ir atom below.[11] Such sp^3 hybridization is possible only in hcp or fcc regions, where every other C atom is placed above a surface Ir atom. In the case of G/Cu(111), we have carried out such study by depositing the atomic hydrogen at room temperature (RT) (using a hot hydrogen (~1900 K) atom beam source) and then cooling the sample to 5 K to acquire the STM data (see Methods for details). The amount of H atoms adsorbed is intentionally diluted, 0.005 ML, to ensure a large average separation between neighbors.

Figure 6a shows a large STM image, revealing both the graphene layer and the underlying Cu(111) surface after the atomic hydrogen exposure. Hydrogen atoms on the graphene layer appear as bright triangular-shaped features pointing to opposite directions depending upon its graphene sublattice adsorption site. Using the graphene transparency to tunneling electrons, we can check the local coupling of the H impurities with the metallic interface following the Cu(111) surface quasiparticles scattering. We observe in Figure 6a the presence of standing wave patterns generated by the existence of intercalated impurities on the Cu(111) surface. Such impurities, appearing as dark round features, always occupy minima of the

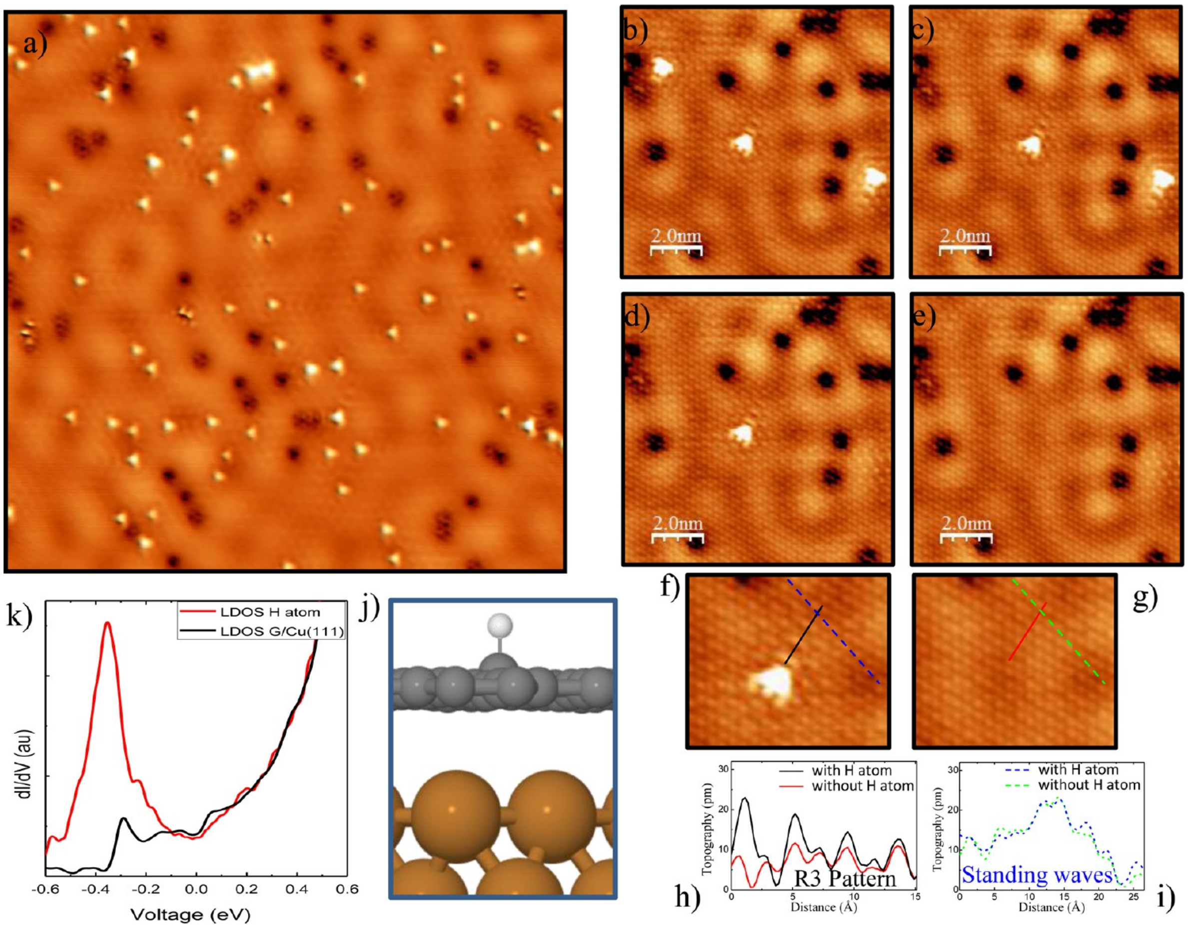

Figure 6. Use of the tunable transparency as a tool to follow the interaction between atomic hydrogen adsorbed onto G/Cu(111). (a) Large-scale STM images showing the general morphology of the G/Cu(111) surface after H deposition. Triangular bright features correspond to single H atoms on the graphene layer. Small dark rounded features are Cu(111) surface impurities. Standing waves from the Cu(111) surface are also observed (V_{bias} = 0.010 V, I_t = 0.2 nA). (b) High resolution STM image showing a 10 × 10 nm^2 sample region with 3 H atoms. (c−e) STM images of the same sample region as in (b) showing that the removal of H atoms does not affect the Cu(111) standing waves patters (V_{bias} = −0.01 V, I_t = 0.5 nA). (f and g) Zoom-in of the central region of images (d and e), respectively, to show the effect of removing a H atom on graphene R3 patterns, see line profiles in (h); and standing waves, see line profiles in (i). (j) Side view of the DFT calculation for the adsorption of a H atom in a $\sqrt{57} \times \sqrt{57}$ moiré. (k) The 5 K STS measurements of the LDOS on a H atom (red curve) and on pristine G/Cu(111) (black curve).

LDOS modulation and act as scattering centers for the Cu(111) surface state. In contrast, the H triangular bright features can be independently found both over bright and dark regions of the Cu(111) standing wave patterns, suggesting a lack of interaction with the Cu(111) surface quasiparticles. But this is not the case when considering the interaction with the graphene overlayer: The high resolution STM image of Figure 6b−e shows that H atoms act as scattering centers for graphene quasiparticles. Thanks to the STM sensitivity to both the overlayer and Cu surface state, R3 patterns originated from the intervalley scattering of graphene quasiparticles are observed, independent of the standing waves underneath.

The absence of a strong H interaction can be unambiguously demonstrated experimentally based on the atomic manipulation capabilities of the STM.[66,67] We can selectively remove H atoms from the graphene surface by gently approaching the STM tip. Figure 6b−e shows how we can subsequently remove 3 H atoms in a controlled way. After each single H atom removal, the same sample region is imaged back to check for any difference arising in the scattering patterns originated by both graphene, R3 patterns, and Cu(111), standing waves patterns, quasiparticles. The sequence of STM images obtained after each H atom removal clearly show that while graphene R3 patterns surrounding H atoms vanish, the Cu(111) standing waves patterns are not affected at all by any H atom removal (see also Figure 6f−i). This confirms that H atoms adsorbed on the graphene layer do not induce any local interaction between the C atoms of the graphene layer and the underlying Cu(111) substrate. Our DFT + D2 calculations support the negligible modification on the G−Cu interaction upon H adsorption. The simulation of the adsorption of a H atom in a $\sqrt{57} \times \sqrt{57}$ moiré (respect to the G) shows that the atomic configuration of the G (see Figure 6j) is very similar to the one obtained on free-standing layers;[38,39,68] moreover, no significant variations either on the average G−Cu distance or the position of Cu atoms are found.

Our results imply that the G/Cu(111) system essentially behaves as an electron-doped graphene layer for atomic hydrogen adsorbates. This can be directly probed by STS experiments. According to theoretical predictions,[38,39,68] adsorbing a single H atom on a graphene layer generates a localized electronic state around the H atom at an energy E_D.

On isolated graphene, where $E_D = E_F$, electron−electron interactions spin-split this state giving rise to a local magnetic moment on the graphene layer. Such magnetic moment is characterized by the presence of two peaks in the LDOS, ascribed to each spin state, and located at both sides of E_F with an energy separation of a few millielectronvolts.[38] On doped enough graphene layers, the energy shift of E_D prevents the spin-polarization of the state, which is predicted to show up in the LDOS as a single peak at the actual E_D energy position.[68] Figure 6k shows STS spectra measured on top of H atoms (red line) and on the Gr/Cu (black line). Above H atoms, the emergence of a single broad peak in the LDOS located around E_D (−0.36 eV) is observed, excluding thus the formation of a H induced magnetic moment, as expected for H adsorption on an electron-doped graphene layer; interestingly, the measure of the LDOS peak energy position after the adsorption of H atoms could be used to determine E_D in some graphene systems. Such single broad electronic resonance around −0.36 eV was observed for all single H atoms independently of their position inside the moiré, which points to a small influence of the moiré superstructure on their properties. The only influence detected was the variation of the resonance height for H atoms on different moiré positions. Our STS data show that for H atoms the only role played by the Cu substrate is to electron-dope the graphene layer, in agreement with the lack of direct coupling observed between the H adsorbates and the metal interface.

Another interesting route to modify graphene properties is the introduction of single C vacancies in graphene layers. Consequently, such C vacancies have been thoroughly investigated both theoretically[38] and by STM.[14,36] When generated in HOPG surfaces,[14] they essentially retain the main properties expected for C vacancies in free-standing graphene.[38] However, it has been shown that the situation is very different for the weakly interacting G/Pt(111) system, where the interaction with the graphene layer strongly increases after the introduction of single carbon vacancies.[36] According to DFT calculations, a strong local interaction between the graphene and substrate develops where the vacancies are located.[36] Thus, C vacancies appears as an optimal system to test the potential of the graphene tunable transparency.

We have deliberately introduced C vacancies into the graphene layer by irradiating the surface with 140 eV Ar^+ ions, which are known to mainly generate singe C vacancies in graphite surfaces and in G/Pt(111).[14,36] Our STM measurements after the irradiation procedure reveal the appearance of almost identical bright features on the previously pristine graphene layer, in a number almost equal to the number of Ar^+ ions impacting the surface, see Figure S7. Because of the graphene tunable transparency, we can probe the impact of the C vacancies both in the graphene layers and in the Cu(111) surface underneath. This is demonstrated in Figure 7a,b, which show exactly the same G/Cu(111) region, with two C vacancies, for high (I = 0.5 nA) and low (I = 0.1 nA) tunneling currents to probe the graphene layer and Cu(111) surface, respectively. When probing the graphene layer, C vacancies appear in STM images as bright protrusions surrounded by R3 patterns, see Figure 7a. When probing the underlying Cu(111) substrate as in Figure 7b, in the position of C vacancies small round features surrounded by Cu(111) standing waves appear (see Figure S7 for a larger overview), which implies that C vacancies located in the graphene layer act as scattering centers for the Cu(111) surface state quasiparticles. This indicates that, contrary to the case of H atoms, C vacancies do strongly interact with the metal substrate underneath.

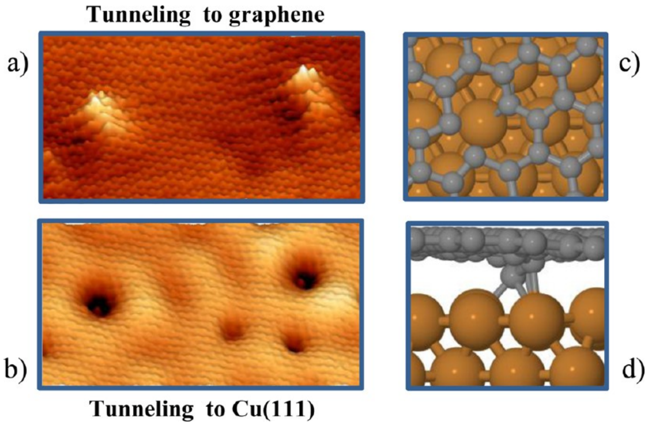

Figure 7. Use of the tunable transparency to follow the interaction between graphene C vacancies and the Cu(111) substrate underneath. (a) STM image showing a G/Cu(111) sample region with two single C vacancies deliberately introduced on the graphene layer by Ar irradiation (V_{bias} = 0.010 V; I = 0.5 nA). (b) Same sample region measured at a lower current (I = 0.1 nA) to probe the underlying Cu(111) surface. C vacancies in graphene act as scattering centers for the Cu(111) surface quasiparticles generating standing waves below them. (c and d) Top (c) and side (d) view of the ball-and-stick model of the atomic structure calculated with DFT of a G monovacancy in the $\sqrt{57} \times \sqrt{57}$ moiré pattern. The characteristic 2 + 1 reconstruction of the C vacancy in graphene is obtained, with two C atoms forming a soft bond and the remaining C atom strongly interacting with the Cu surface.

We have also carried out a DFT simulation of a monovacancy in the G on Cu on the $\sqrt{57} \times \sqrt{57}$ moiré pattern (see Methods for details). The vacancy reconstructs with the same Jahn−Teller distortion that has been identified in free-standing graphene,[38] with two of the three C atoms forming a soft bond. The reactive dangling bond of the third C atom strongly interacts with the underneath metal. The bonds between the carbon atom and the Cu surface atoms induce a significant out-of-plane distortion of the G layer in the neighborhood of the vacancy (more than 1 Å). The final structure is very similar to the one found for single-atom vacancies in G on Pt.[36] Adsorbates are well recognized as scattering centers for the Cu surface state. As confirmed by our STM measurements, due to the strong interaction with the substrate, this carbon atom acts effectively as an adsorbate for the Cu surface inducing the observed standing wave pattern.

The case of single C vacancies in graphene layers appears as an optimal system to test the potential of the graphene tunable transparency. When generated in HOPG surfaces,[14] they essentially retain the main properties expected for C vacancies in free-standing graphene.[38] However, it has been shown that for the weakly interacting G/Pt(111) system, the interaction with the graphene layer strongly increases after the introduction of single carbon vacancies in the graphene layer.[36] According to theoretical calculations, a strong local interaction between the graphene and substrate develops where the atomic C vacancies are located.

CONCLUSIONS

We show that the selective modification of the tunneling parameters in STM experiments opens the possibility to simultaneously characterize by STM/STS a graphene layer and the substrate underneath. By performing low temperature STS/STM experiments on a graphene monolayer grown on a Cu(111) surface, we show that this graphene tunable transparency enables the accurate measure of the local electronic properties of both graphene and Cu(111) surface at the same sample region and within the same energy range. This offers a complete picture of the mutual interactions among the different system parts. The exceptional agreement between the STM results and our ARPES data excludes tip artifacts and strengthens the confidence in the obtained results. More so since our experimental findings are complemented by DFT−vdW calculations, which offer a realistic explanation to the graphene tunable transparency in terms of the different wave functions that spill out of the graphene and Cu(111) surface state. The large experimental data set is key to the accurate theoretical description of weakly interacting graphene/substrate systems.

There are a number of recent references where graphene on noble metals has been studied with either STM-based or photoemission techniques, including G/Ag (using STS),[69] G nanoflakes on Au (with STM/STS and FT-STS),[70] and a previous work on G/Cu (ARPES).[20,71] They do exploit the interplay between the G and the metal surface state confirming that our method has a general applicability not limited to the particular case of G/Cu. Moreover, the transparency of graphene in tunneling experiments is not restricted to metals since, for example, it has also been noticed for epitaxial graphene grown on SiC substrates where the interface with SiC was imaged.[27−29]

In summary, the combination of two complementary techniques like STS and ARPES, the systematic study of the changes in both the G and metal surface states, and the insight provided by our theoretical simulations, which help to clarify the origin of the tunable transparency, conclusively prove the general applicability of our method.

The versatility of our approach is further exploited by extending the method to modified graphene layers. In particular, we prove that the diluted adsorption of atomic H on top of the graphene layer on Cu(111) does not increase the local coupling between the C atoms surrounding the H adsorbates and the metal underneath. We also exclude any magnetism associated with the H adsorption, reported in the case of free-standing graphene. In contrast, C vacancies introduced in the graphene layer do strongly interact with the metal substrate underneath.

Unravelling the mechanism behind the tunable transparency has the prospect of becoming a powerful tool to study weakly interactive systems. The possibility of characterizing independently each system part is key to achieve a detailed understanding of the local interactions, in particular in the vicinity of intercalated or adsorbed particles.

METHODS

STM: Sample Preparation. To grow monolayer graphene on Cu(111), we have used a technique developed by some of us[31] consisting of the thermal decomposition of low energy ethylene ions irradiated on a hot copper surface, which allows the growth of very large graphene domains free of defects. This technique consists of three steps: (1) preparation of clean Cu(111) surface by the standard method of Ar^+ bombardment and annealing cycles; (2) ethylene irradiation, with an accelerated ion energy of 0.5 keV, keeping the Cu(111) substrate at around 800 °C; and (3) further annealing of the sample for 10 min at around 900°. We deposited atomic hydrogen by the thermal dissociation of H_2 on a homemade hot hydrogen atom beam source. A molecular H_2 beam is passed through a hot W filament held at 1900 K. The pristine graphite surface is placed 10 cm away from the filament and held at RT during atomic H deposition. H_2 pressure is regulated by a leak valve and fixed to 3×10^{-7} Torr as measured in the preparation chamber for the present experiments. A low final coverage, of 0.2 H atoms/nm^2 (or equivalently, 0.005 ML; 1 ML = 38 atoms/nm^2 = 3.8×10^{15} atoms/cm^2, referred to carbon atoms in graphene layers), is to ensure an average first neighbors H−H distance ≥1 nm. Control experiments where the sample was exposed to the same 3×10^{-7} Torr H_2 pressure and deposition times keeping the W filament cold and experiments with the W filament at the same 1900 K temperature without molecular H_2 did not show any trace of H (no triangular bright features could be observed) or any other atomic adsorbate on the surface. C vacancies where introduced in the graphene layer by irradiating the surface with 140 eV Ar^+ ions, following exactly the same procedure as to generate single C vacancies in graphite surfaces and in G/Pt(111).[14,36] A key point of the present work is the atomistic control of the samples, which was obtained by performing all the preparation procedures and measurements under UHV conditions (during the whole process−preparation of graphene/Cu(111) sample → imaging pristine G/Cu(111) sample → depositing H atoms (or introducing C vacancies) on it → and imaging it again, the sample was always maintained in the same UHV system).

STM: STS Measurements. A homemade LT-STM operating at 5 K in UHV[14] and using the WSxM program[72] was used to characterize the samples. Our atomically resolved STM images reveal the growth of high quality graphene films presenting different orientations with respect to the Cu(111) surface, as reflected by the presence of moiré patterns with different periodicities (Figure S1). Besides the topographic characterization, when operated in its spectroscopic mode, STM/STS also provides information on the local electronic properties of the surface with atomic resolution and high energy accuracy (2 meV in the present case). The differential conductance (dI/dV) maps measured by STM at energies near E_F are closely related to the LDOS(E) of the sample under the tip apex position. Thus, dI/dV conductance images essentially show maps corresponding to spatial variations of the sample LDOS. By measuring dI/dV maps at different energies, one can obtain the energy dispersion $E(k)$ for a specific region of the sample, see Supporting Information for further details.

The actual procedure to selectively change the tip state was the following: We first imaged an specific G/Cu(111) region with a given tip, *i.e.*, a tip probing either Cu surface states or graphene states. Then, we moved ∼500 nm away from this region to modify the tip apex by the controlled indentation of the STM tip onto the substrate without affecting the region of interest. Typical indentation values were as follows: z-displacement ∼2−4 nm, bias voltage ∼1−2 V. After each indentation experiment, we acquired a dI/dV spectrum to check the tip state. We found that by acquiring an STS spectrum we could quickly identify which kind of tip we had: tips probing graphene states have a reduced DOS in the vicinity of E_F (possibly due to some contamination of the tip apex with electronegative impurities), while tips sensing Cu(111) surface states clearly see the onset of the Cu(111) surface state with a featureless DOS close to E_F (as expected from a purely metallic tip), see Figure S13. We systematically repeated this procedure until we obtained the desired tip-apex change. The exact number of indentations required varied from tip to tip, but after a few repetitions, it was always possible to obtain the desired tip state. Then, we moved back to the initial region and measured it again with the modified tip to fully characterize it.

ARPES Experiments. To grow the graphene monolayer on Cu(111), we have used the standard ethylene cracking method reaching temperatures close to the Cu melting point.[20,41] We achieved homogeneous, single domains extending over large sample areas. The data in Figure 5 indicate the presence of a dominant graphene domain over the area sampled by the light spot size of 0.25 mm^2.

Our home laboratory angle resolved photoemission (ARPES) setup consists of a display type hemispherical analyzer (Phoibos150) with an energy/angle resolution of 40 meV/0.1° and a monochromatized source Helium I ($h\nu$ = 21.2 eV) source. The channel plate slit lies along the rotation axis of the manipulator. All the presented data were recorded approximately at 180 K.

DFT Calculations. We have calculated all the structural and electronic properties using DFT as implemented in the VASP code.[55] For these calculations, we employed the PBE functional[51] empirically corrected to include van der Waals interactions (using the D2 Grimme approach),[52] projector augmented wave (PAW) pseudopotentials,[56] and a plane-wave cutoff of 400 eV. For the calculation with the 1 × 1 surface cell, we have used 15 Cu layers and the G (for a total of 17 atoms) with a vacuum space of ∼10−9.5 Å. For the calculations on the $(\sqrt{57} \times \sqrt{57})$-G moiré pattern (corresponding to a $\sqrt{52} \times \sqrt{52}$ unit cell for Cu), we have adsorbed a G layer with 114 C on a slab with 4 Cu layers ($52 \times 4 + 114 = 322$ atoms in the unit cell), leaving a vacuum space of ∼10−9.5 Å. Both the H adsorption and the monovacancy calculations were performed with this supercell. In our calculations, we decided to fix the size of the supercell to match the relaxed Cu lattice ($a_0 = 2.57$ Å) in order to accurately describe the Cu surface state. The final structures correspond to energies converged better than 10^{-5} eV/atom and forces smaller than 0.02 eV/Å. We have used a 35 × 35 or 3 × 3 Γ-centered Monkhorst−Pack grid to make the relaxation of the structures on the 1 × 1 or $\sqrt{57} \times \sqrt{57}$ unit cell, respectively. The effect of the G−Cu separation is studied calculating the electronic structure displacing the G from the atomic structure of the relaxed G on Cu. Calculations of the charge distribution and the work functions are carried out with finer convergence criteria: plane-wave cutoff of 600 eV, ∼20 Å of vacuum and a 51 × 51 Γ-centered Monkhorst−Pack grid. Dipole correction to subtract intercell interactions is required for the calculation of the work functions.

STM Simulations. We use a nonequilibrium Green's function formalism to evaluate the currents,[58] using the OPENMX code[73] with the PBE functional[51] to map the Hamiltonian into a local orbital basis. We have considered two different models for tip apexes: A pure Cu (111)-oriented tip with 10 atoms (Cu10 tip), and an O-contaminated tip, where we replace the Cu atom at the apex by an O atom (CuO tip). All the simulations include the contribution to the current of multiple scattering processes.[58] The system used to explain the real Cu-standing waves observed in the experiments is composed of a 9 × 1 Cu surface cell with 15 Cu layers (153 atoms) and a G layer placed at the correct G−Cu distance (3.4 Å) to reproduce the experiments. One of the Cu surface atoms has been substituted by an oxygen atom at the same atomic position, making a line defect that yields a spatial modulation on the Cu surface state. This is just a model to induce a perturbation of the surface charge density, not a realistic defect structure, and thus, no attempt of simulating the real configuration of this defect has been made by relaxation of this structure (atomic positions have been kept fixed). A double-ζ (s2p2d2) Cu orbital basis set with a cutoff radio of 10 au is required to get a correct description of the surface state. STM profiles simulate constant current scans with a bias of −100 mV (current to sample filled states) and they are done with a 9 × 75 k-mesh.

ASSOCIATED CONTENT

Ⓢ Supporting Information

The Supporting Information is available free of charge on the ACS Publications website at DOI: 10.1021/acsnano.6b00322.

> STM characterization of the general morphology of the graphene/Cu(111) samples, STM characterization of 2D electronic states, large view of STM/STS data, STM/STS measurements of the graphene electron doping, theoretical description of the dispersive (van der Waals) interactions, charge transfer and level alignment, simulation results of the $\sqrt{57} \times \sqrt{57}$ moiré pattern, further details of the explanation of graphene tunable transparency, Figures S1−S12 (PDF)

AUTHOR INFORMATION

Corresponding Author

*E-mail: ivan.brihuega@uam.es.

Notes

The authors declare no competing financial interest.

ACKNOWLEDGMENTS

We acknowledge financial support from Spanish Grant MAT2013-41636-P, PCIN-2015-030, MAT2011-23627, MAT2011-26534, MAT2013-6593-C6-4-P, MAT2014-54484-P, MDM-2014-0377, CSD2010-00024 (MINECO, Spain) and S2009/MAT-1467 (CAM, Spain), IT621-13 (Basque Government) the European Union structural funds and the Comunidad de Madrid MAD2D-CM Program (S2013/MIT-3007) and the European Union FLAG-ERA program. P.P. was supported by the Ramón y Cajal program. A.J.M.-G. was supported by the Marie Curie program. Computer time provided by the Spanish Supercomputing Network (RES) in the Barcelona Supercomputer Center (MareNostrum III) and the CesViMa (Magerit) is gratefully acknowledged.

REFERENCES

(1) Ohta, T.; Bostwick, A.; Seyller, T.; Horn, K.; Rotenberg, E. Controlling the Electronic Structure of Bilayer Graphene. *Science* **2006**, *313*, 951−954.

(2) Ohta, T.; Bostwick, A.; Mcchesney, J. L.; Seyller, T.; Horn, K.; Rotenberg, E. Interlayer Interaction And Electronic Screening in Multilayer Graphene Investigated with Angle-Resolved Photoemission Spectroscopy. *Phys. Rev. Lett.* **2007**, *98*, 206802.

(3) Zhou, S. Y.; Gweon, G. H.; Fedorov, A. V.; First, P. N.; De Heer, W. A.; Lee, D. H.; Guinea, F.; Neto, A. H. C.; Lanzara, A. Substrate-Induced Bandgap Opening in Epitaxial Graphene. *Nat. Mater.* **2007**, *6*, 770−775.

(4) Craciun, M. F.; Russo, S.; Yamamoto, M.; Oostinga, J. B.; Morpurgo, A. F.; Thrucha, S. Trilayer Graphene is a Semimetal with a Gate-Tunable Band Overlap. *Nat. Nanotechnol.* **2009**, *4*, 383−388.

(5) Giovannetti, G.; Khomyakov, P. A.; Brocks, G.; Karpan, V. M.; Van Den Brink, J.; Kelly, P. J. Doping Graphene with Metal Contacts. *Phys. Rev. Lett.* **2008**, *101*, 026803.

(6) Decker, R.; Brede, J.; Atodiresei, N.; Caciuc, V.; Blugel, S.; Wiesendanger, R. Atomic-Scale Magnetism of Cobalt-Intercalated Graphene. *Phys. Rev. B: Condens. Matter Mater. Phys.* **2013**, *87*, No. 041403(R).

(7) Wintterlin, J.; Bocquet, M. L. Graphene on Metal Surfaces. *Surf. Sci.* **2009**, *603*, 1841−1852.

(8) Pletikosic, I.; Kralj, M.; Pervan, P.; Brako, R.; Coraux, J.; N'Diaye, A. T.; Busse, C.; Michely, T. Dirac Cones And Minigaps For Graphene on Ir(111). *Phys. Rev. Lett.* **2009**, *102*, 056808.

(9) Hwang, C.; Siegel, D. A.; Mo, S. K.; Regan, W.; Ismach, A.; Zhang, Y. G.; Zettl, A.; Lanzara, A. Fermi Velocity Engineering in Graphene By Substrate Modification. *Sci. Rep.* **2012**, *2*, 590.

(10) Heersche, H. B.; Jarillo-Herrero, P.; Oostinga, J. B.; Vandersypen, L. M. K.; Morpurgo, A. F. Bipolar Supercurrent in Graphene. *Nature* **2007**, *446*, 56−59.

(11) Balog, R.; Jorgensen, B.; Nilsson, L.; Andersen, M.; Rienks, E.; Bianchi, M.; Fanetti, M.; Laegsgaard, E.; Baraldi, A.; Lizzit, S.; Sljivancanin, Z.; Besenbacher, F.; Hammer, B.; Pedersen, T. G.; Hofmann, P.; Hornekaer, L. Bandgap Opening in Graphene Induced by Patterned Hydrogen Adsorption. *Nat. Mater.* **2010**, *9*, 315−319.

(12) Zhao, L. Y.; He, R.; Rim, K. T.; Schiros, T.; Kim, K. S.; Zhou, H.; Gutierrez, C.; Chockalingam, S. P.; Arguello, C. J.; Palova, L.; Nordlund, D.; Hybertsen, M. S.; Reichman, D. R.; Heinz, T. F.; Kim, P.; Pinczuk, A.; Flynn, G. W.; Pasupathy, A. N. Visualizing Individual Nitrogen Dopants in Monolayer Graphene. *Science* **2011**, *333*, 999−1003.

(13) Nair, R. R.; Tsai, I. L.; Sepioni, M.; Lehtinen, O.; Keinonen, J.; Krasheninnikov, A. V.; Neto, A. H. C.; Katsnelson, M. I.; Geim, A. K.; Grigorieva, I. V. Dual Origin of Defect Magnetism in Graphene and its Reversible Switching By Molecular Doping. *Nat. Commun.* **2013**, *4*, 2010.

(14) Ugeda, M. M.; Brihuega, I.; Guinea, F.; Gomez-Rodriguez, J. M. Missing Atom as a Source of Carbon Magnetism. *Phys. Rev. Lett.* **2010**, *104*, 096804.

(15) Riedl, C.; Coletti, C.; Iwasaki, T.; Zakharov, A. A.; Starke, U. Quasi-Free-Standing Epitaxial Graphene on SiC Obtained by Hydrogen Intercalation. *Phys. Rev. Lett.* **2009**, *103*, 246804.

(16) Gierz, I.; Suzuki, T.; Weitz, R. T.; Lee, D. S.; Krauss, B.; Riedl, C.; Starke, U.; Hochst, H.; Smet, J. H.; Ast, C. R.; Kern, K. Electronic Decoupling of an Epitaxial Graphene Monolayer by Gold Intercalation. *Phys. Rev. B: Condens. Matter Mater. Phys.* **2010**, *81*, 235408.

(17) Varykhalov, A.; Sanchez-Barriga, J.; Shikin, A. M.; Biswas, C.; Vescovo, E.; Rybkin, A.; Marchenko, D.; Rader, O. Electronic and Magnetic Properties of Quasifreestanding Graphene on Ni. *Phys. Rev. Lett.* **2008**, *101*, 157601.

(18) Calleja, F.; Ochoa, H.; Garnica, M.; Barja, S.; Navarro, J. J.; Black, A.; Otrokov, M. M.; Chulkov, E. V.; Arnau, A.; De Parga, A. L. V.; Guinea, F.; Miranda, R. Spatial Variation of a Giant Spin-Orbit Effect Induces Electron Confinement in Graphene on Pb Islands. *Nat. Phys.* **2015**, *11*, 43−47.

(19) Gruneis, A.; Vyalikh, D. V. Tunable Hybridization Between Electronic States of Graphene and a Metal Surface. *Phys. Rev. B: Condens. Matter Mater. Phys.* **2008**, *77*, 193401.

(20) Walter, A. L.; Nie, S.; Bostwick, A.; Kim, K. S.; Moreschini, L.; Chang, Y. J.; Innocenti, D.; Horn, K.; Mccarty, K. F.; Rotenberg, E. Electronic Structure of Graphene on Single-Crystal Copper Substrates. *Phys. Rev. B: Condens. Matter Mater. Phys.* **2011**, *84*, 195443.

(21) Rutter, G. M.; Crain, J. N.; Guisinger, N. P.; Li, T.; First, P. N.; Stroscio, J. A. Scattering and Interference in Epitaxial Graphene. *Science* **2007**, *317*, 219−222.

(22) Li, G. H.; Luican, A.; Dos Santos, J.; Neto, A. H. C.; Reina, A.; Kong, J.; Andrei, E. Y. Observation of Van Hove Singularities in Twisted Graphene Layers. *Nat. Phys.* **2010**, *6*, 109−113.

(23) Zhang, Y. B.; Brar, V. W.; Girit, C.; Zettl, A.; Crommie, M. F. Origin of Spatial Charge Inhomogeneity in Graphene. *Nat. Phys.* **2009**, *5*, 722−726.

(24) Hashimoto, A.; Suenaga, K.; Gloter, A.; Urita, K.; Iijima, S. Direct Evidence For Atomic Defects in Graphene Layers. *Nature* **2004**, *430*, 870−873.

(25) Meyer, J. C.; Geim, A. K.; Katsnelson, M. I.; Novoselov, K. S.; Booth, T. J.; Roth, S. The Structure of Suspended Graphene Sheets. *Nature* **2007**, *446*, 60−63.

(26) Gomez-Navarro, C.; Meyer, J. C.; Sundaram, R. S.; Chuvilin, A.; Kurasch, S.; Burghard, M.; Kern, K.; Kaiser, U. Atomic Structure of Reduced Graphene Oxide. *Nano Lett.* **2010**, *10*, 1144−1148.

(27) Berger, C.; Song, Z. M.; Li, X. B.; Wu, X. S.; Brown, N.; Naud, C.; Mayou, D.; Li, T. B.; Hass, J.; Marchenkov, A. N.; Conrad, E. H.; First, P. N.; De Heer, W. A. Electronic Confinement and Coherence in Patterned Epitaxial Graphene. *Science* **2006**, *312*, 1191−1196.

(28) Rutter, G. M.; Guisinger, N. P.; Crain, J. N.; Jarvis, E. A. A.; Stiles, M. D.; Li, T.; First, P. N.; Stroscio, J. A. Imaging the Interface of Epitaxial Graphene with Silicon Carbide *via* Scanning Tunneling Microscopy. *Phys. Rev. B: Condens. Matter Mater. Phys.* **2007**, *76*, 235416.

(29) Brar, V. W.; Zhang, Y.; Yayon, Y.; Ohta, T.; Mcchesney, J. L.; Bostwick, A.; Rotenberg, E.; Horn, K.; Crommie, M. F. Scanning Tunneling Spectroscopy of Inhomogeneous Electronic Structure in Monolayer and Bilayer Graphene on SiC. *Appl. Phys. Lett.* **2007**, *91*, 122102.

(30) Jeon, I.; Yang, H.; Lee, S. H.; Heo, J.; Seo, D. H.; Shin, J.; Chung, U. I.; Kim, Z. G.; Chung, H. J.; Seo, S. Passivation of Metal Surface States: Microscopic Origin For Uniform Mono Layer Graphene by low Temperature Chemical Vapor Deposition. *ACS Nano* **2011**, *5*, 1915−1920.

(31) Martinez-Galera, A. J.; Brihuega, I.; Gomez-Rodriguez, J. M. Ethylene Irradiation: A New Route to Grow Graphene on Low Reactivity Metals. *Nano Lett.* **2011**, *11*, 3576−3580.

(32) Altenburg, S. J.; Kroger, J.; Wehling, T. O.; Sachs, B.; Lichtenstein, A. I.; Berndt, R. Local Gating of an Ir(111) Surface Resonance by Graphene Islands. *Phys. Rev. Lett.* **2012**, *108*, 206805.

(33) Bartelt, N. C.; Mccarty, K. F. Graphene Growth on Metal Surfaces. *MRS Bull.* **2012**, *37*, 1158.

(34) Li, X. S.; Cai, W.; An, J.; Kim, S.; Nah, J.; Yang, D.; Piner, R.; Velamakanni, A.; Jung, I.; Tutuc, E.; Banerjee, S. K.; Colombo, L.; Ruoff, R. S. Large-Area Synthesis of High-Quality and Uniform Graphene Films on Copper Foils. *Science* **2009**, *324*, 1312−1314.

(35) Bae, S.; Kim, H.; Lee, Y.; Xu, X. F.; Park, J. S.; Zheng, Y.; Balakrishnan, J.; Lei, T.; Kim, H. R.; Song, Y. I.; Kim, Y. J.; Kim, K. S.; Ozyilmaz, B.; Ahn, J. H.; Hong, B. H.; Iijima, S. Roll-To-Roll Production of 30-Inch Graphene Films for Transparent Electrodes. *Nat. Nanotechnol.* **2010**, *5*, 574−578.

(36) Ugeda, M. M.; Fernandez-Torre, D.; Brihuega, I.; Pou, P.; Martínez-Galera, A. J.; Perez, R.; Gómez-Rodríguez, J. M. Point Defects on Graphene on Metals. *Phys. Rev. Lett.* **2011**, *107*, 116803.

(37) Rusponi, S.; Papagno, M.; Moras, P.; Vlaic, S.; Etzkorn, M.; Sheverdyaeva, P. M.; Pacile, D.; Brune, H.; Carbone, C. Highly Anisotropic Dirac Cones in Epitaxial Graphene Modulated by an Island Superlattice. *Phys. Rev. Lett.* **2010**, *105*, 246803.

(38) Yazyev, O. V.; Helm, L. Defect-Induced Magnetism in Graphene. *Phys. Rev. B: Condens. Matter Mater. Phys.* **2007**, *75*, 125408.

(39) Boukhvalov, D. W.; Katsnelson, M. I.; Lichtenstein, A. I. Hydrogen on Graphene: Electronic Structure, Total Energy, Structural Distortions and Magnetism from First-Principles Calculations. *Phys. Rev. B: Condens. Matter Mater. Phys.* **2008**, *77*, 035427.

(40) Elias, D. C.; Nair, R. R.; Mohiuddin, T. M. G.; Morozov, S. V.; Blake, P.; Halsall, M. P.; Ferrari, A. C.; Boukhvalov, D. W.; Katsnelson, M. I.; Geim, A. K.; Novoselov, K. S. Control of Graphene's Properties by Reversible Hydrogenation: Evidence for Graphane. *Science* **2009**, *323*, 610−613.

(41) Gao, L.; Guest, J. R.; Guisinger, N. P. Epitaxial Graphene on Cu(111). *Nano Lett.* **2010**, *10*, 3512−3516.

(42) Nie, S.; Wofford, J. M.; Bartelt, N. C.; Dubon, O. D.; Mccarty, K. F. Origin of the Mosaicity in Graphene Grown on Cu(111). *Phys. Rev. B: Condens. Matter Mater. Phys.* **2011**, *84*, 155425.

(43) Brihuega, I.; Mallet, P.; Bena, C.; Bose, S.; Michaelis, C.; Vitali, L.; Varchon, F.; Magaud, L.; Kern, K.; Veuillen, J. Y. Quasiparticle Chirality in Epitaxial Graphene Probed at the Nanometer Scale. *Phys. Rev. Lett.* **2008**, *101*, 206802.

(44) Mallet, P.; Brihuega, I.; Bose, S.; Ugeda, M. M.; Gomez-Rodriguez, J. M.; Kern, K.; Veuillen, J. Y. Role of Pseudospin in Quasiparticle Interferences in Epitaxial Graphene Probed by High-Resolution Scanning Tunneling Microscopy. *Phys. Rev. B: Condens. Matter Mater. Phys.* **2012**, *86*, 045444.

(45) Park, J. Y.; Ham, U. D.; Kahng, S. J.; Kuk, Y.; Miyake, K.; Hata, K.; Shigekawa, H. Modification of Surface-State Dispersion upon Xe Adsorption: A Scanning Tunneling Microscope Study. *Phys. Rev. B: Condens. Matter Mater. Phys.* **2000**, *62*, 16341−16344.

(46) Repp, J.; Meyer, G.; Rieder, K. H. Snell's Law for Surface Electrons: Refraction of an Electron Gas Imaged in Real Space. *Phys. Rev. Lett.* **2004**, *92*, 036803.

(47) Grimme, S. Density Functional Theory With London Dispersion Corrections. *Wires Comput. Mol. Sci.* **2011**, *1*, 211−228.

(48) Klimes, J.; Michaelides, A. Perspective: Advances and Challenges in Treating Van der Waals Dispersion Forces in Density Functional Theory. *J. Chem. Phys.* **2012**, *137*, 120901.

(49) Batzill, M. The Surf. Sci. of Graphene: Metal Interfaces, CVD Synthesis, Nanoribbons, Chemical Modifications, and Defects. *Surf. Sci. Rep.* **2012**, *67*, 83−115.

(50) Iannuzzi, M.; Kalichava, I.; Ma, H.; Leake, S. J.; Zhou, H.; Li, G.; Zhang, Y.; Bunk, O.; Gao, H.; Hutter, J.; Willmott, P. R.; Greber, T. Moiré Beatings in Graphene on Ru(0001). *Phys. Rev. B: Condens. Matter Mater. Phys.* **2013**, *88*, 125433.

(51) Perdew, J. P.; Burke, K.; Ernzerhof, M. Generalized Gradient Approximation Made Simple. *Phys. Rev. Lett.* **1996**, *77*, 3865−3868.

(52) Grimme, S. Semiempirical GGA-Type Density Functional Constructed with a Long-Range Dispersion Correction. *J. Comput. Chem.* **2006**, *27*, 1787−1799.

(53) Grimme, S.; Antony, J.; Ehrlich, S.; Krieg, H. A Consistent and Accurate ab Initio Parametrization of Density Functional Dispersion Correction (DFT-D) For the 94 Elements H-Pu. *J. Chem. Phys.* **2010**, *132*, 154104.

(54) Klimes, J.; Bowler, D. R.; Michaelides, A. van der Waals Density Functionals Applied to Solids. *Phys. Rev. B: Condens. Matter Mater. Phys.* **2011**, *83*, 195131.

(55) Kresse, G.; Furthmüller, J. Efficient Iterative Schemes for ab Initio Total-Energy Calculations Using A Plane-Wave Basis set. *Phys. Rev. B: Condens. Matter Mater. Phys.* **1996**, *54*, 11169.

(56) Kresse, G.; Joubert, D. From Ultrasoft Pseudopotentials to the Projector Augmented-Wave Method. *Phys. Rev. B: Condens. Matter Mater. Phys.* **1999**, *59*, 1758.

(57) Khomyakov, P. A.; Giovannetti, G.; Rusu, P. C.; Brocks, G.; van den Brink, J.; Kelly, P. J. First-Principles Study of the Interaction and Charge Transfer Between Graphene and Metals. *Phys. Rev. B: Condens. Matter Mater. Phys.* **2009**, *79*, 195425.

(58) Chen, C. J. *Introduction to Scanning Tunneling Microscopy*, 2nd ed.; University Press, 2008.

(59) Blanco, J. M.; Flores, F.; Perez, R. STM-Theory: Image Potential, Chemistry and Surface Relaxation. *Prog. Surf. Sci.* **2006**, *81*, 403−443.

(60) Mönig, H.; Todorović, M.; Baykara, M. Z.; Schwendemann, T. C.; Rodrigo, L.; Altman, E. I.; Perez, R.; Schwarz, U. D. Understanding Scanning Tunneling Microscopy Contrast Mechanisms on Metal Oxides: a Case Study. *ACS Nano* **2013**, *7*, 10233.

(61) Hollen, S. M.; Gambrel, G. A.; Tjung, S. J.; Santagata, N. M.; Johnston-Halperin, E.; Gupta, J. A. Modification of Electronic Surface States by Graphene Islands on Cu(111). *Phys. Rev. B: Condens. Matter Mater. Phys.* **2015**, *91*, 195425.

(62) Ondráček, M.; Pou, P.; Rozsíval, V.; González, C.; Jelínek, P.; Pérez, R. Forces and Currents in Carbon Nanostructures: are we Imaging Atoms? *Phys. Rev. Lett.* **2011**, *107*, 176101.

(63) Paniago, R.; Matzdorf, R.; Meister, G.; Goldmann, A. Temperature-Dependence of Shockley-Type Surface-Energy Bands on Cu(111), Ag(111) and Au(111). *Surf. Sci.* **1995**, *336*, 113−122.

(64) Reinert, F.; Nicolay, G.; Schmidt, S.; Ehm, D.; Hufner, S. Direct Measurements of the L-Gap Surface States on the (111) Face of Noble Metals by Photoelectron Spectroscopy. *Phys. Rev. B: Condens. Matter Mater. Phys.* **2001**, *63*, 115415.

(65) Mccreary, K. M.; Swartz, A. G.; Han, W.; Fabian, J.; Kawakami, R. K. Magnetic Moment Formation in Graphene Detected by Scattering of pure spin Currents. *Phys. Rev. Lett.* **2012**, *109*, 186604.

(66) Eigler, D. M.; Schweizer, E. K. Positioning Single Atoms with A Scanning Tunneling Microscope. *Nature* **1990**, *344*, 524−526.

(67) Shen, T. C.; Wang, C.; Abeln, G. C.; Tucker, J. R.; Lyding, J. W.; Avouris, P.; Walkup, R. E. Atomic-Scale Desorption Through Electronic and Vibrational-Excitation Mechanisms. *Science* **1995**, *268*, 1590−1592.

(68) Yndurain, F. Effect of Hole Doping on the Magnetism of Point Defects in Graphene: a Theoretical Study. *Phys. Rev. B: Condens. Matter Mater. Phys.* **2014**, *90*, 245420.

(69) Jolie, W.; Craes, F.; Busse, C. Graphene on Weakly Interacting Metals: Dirac States *Versus* Surface States. *Phys. Rev. B: Condens. Matter Mater. Phys.* **2015**, *91*, 115419.

(70) Leicht, P.; Zielke, L.; Bouvron, S.; Moroni, R.; Voloshina, E.; Hammerschmidt, L.; Dedkov, Y. S.; Fonin, M. *In Situ* Fabrication of Quasi-Free-Standing Epitaxial Graphene Nanoflakes on Gold. *ACS Nano* **2014**, *8*, 3735.

(71) Gottardi, S.; MüLler, K.; Bignardi, L.; Moreno-López, J. C.; Pham, T. A.; Ivashenko, O.; Yablonskikh, M.; Barinov, A.; BjöRk, J.; Rudolf, P.; StöHr, M. Comparing Graphene Growth on Cu(111) *Versus* Oxidized Cu(111). *Nano Lett.* **2015**, *15*, 917−922.

(72) Horcas, I.; Fernández, R.; Gómez-Rodríguez, J. M.; Colchero, J.; Gómez-Herrero, J.; Baró, A. M. WSXM: A Software For Scanning Probe Microscopy and a tool for Nanotechnology. *Rev. Sci. Instrum.* **2007**, *78*, 013705.

(73) Ozaki, T. Variationally Optimized Atomic Orbitals for Large-Scale Electronic Structures. *Phys. Rev. B: Condens. Matter Mater. Phys.* **2003**, *67*, 155108.